2021

Biological resurfacing in a canine model of hip osteoarthritis

Bradley T Estes

Masataka Enomoto

Franklin T Moutos

Megan A Carson

Jeffrey M Toth

See next page for additional authors

Authors

Bradley T Estes, Masataka Enomoto, Franklin T Moutos, Megan A Carson, Jeffrey M Toth, Peter Eggert, Jonathan Stallrich, Vincent P Willard, Deborah J Veis, Dianne Little, Farshid Guilak, and B Duncan X Lascelles

HEALTH AND MEDICINE

Biological resurfacing in a canine model of hip osteoarthritis

Bradley T. Estes[1]*†, Masataka Enomoto[2†], Franklin T. Moutos[1], Megan A. Carson[3], Jeffrey M. Toth[4], Peter Eggert[4], Jonathan Stallrich[5], Vincent P. Willard[1], Deborah J. Veis[6,7,8], Dianne Little[9], Farshid Guilak[1,7,10,11]*‡, B. Duncan X. Lascelles[2,12,13,14]*‡

Articular cartilage has unique load-bearing properties but has minimal capacity for intrinsic repair. Here, we used three-dimensional weaving, additive manufacturing, and autologous mesenchymal stem cells to create a tissue-engineered, bicomponent implant to restore hip function in a canine hip osteoarthritis model. This resorbable implant was specifically designed to function mechanically from the time of repair and to biologically integrate with native tissues for long-term restoration. A massive osteochondral lesion was created in the hip of skeletally mature hounds and repaired with the implant or left empty (control). Longitudinal outcome measures over 6 months demonstrated that the implant dogs returned to normal preoperative values of pain and function. Anatomical structure and functional biomechanical properties were also restored in the implanted dogs. Control animals never returned to normal and exhibited structurally deficient repair. This study provides clinically relevant evidence that the bicomponent implant may be a potential therapy for moderate hip osteoarthritis.

INTRODUCTION

Osteoarthritis (OA) is a degenerative disease affecting all components of the joint, characterized by progressive damage to the articular cartilage and underlying bone. While the primary treatment for end-stage OA is a total joint replacement, long-term follow-up studies show that up to one-third of patients under the age of 40 at the time of total hip arthroplasty have loosening or excessive wear problems later in life (*1*). Thus, any procedures that serve to postpone joint replacement and preserve the joint would have a substantial clinical benefit. However, alternative biologic techniques, such as osteochondral transfer or microfracture procedures, are ineffective for larger lesions (*2*, *3*). Second-generation autologous chondrocyte implantation or matrix-assisted chondrocyte implantation procedures are not approved for use outside the knee joint and report an almost 30% failure rate within 9 years in young patients (*4*–*6*). There is a need for improved techniques, implants, and procedures to effectively treat the disease or, at a minimum, delay the progression of OA to the point at which the patients are better candidates for a hip arthroplasty procedure.

In our previous work, we have developed a unique cartilage repair implant using a textile manufacturing process of three-dimensional (3D) orthogonal weaving to form a construct that is biomechanically and biologically designed for cartilage repair (*7*–*11*). One of the principal advantages of this biomimetic structure is that it enables the implantation of a device that has been optimized to support the loads in the joint while providing a conduit for endogenous cell infiltration, tissue synthesis, and integration with native tissues for long-term functional support (*12*). This approach is in direct contrast to the use of many biomaterials used to date for cartilage tissue engineering, which do not have the mechanical properties and load-bearing characteristics of native cartilage until significant matrix deposition has occurred over time. The basis of this technology is a 3D "microweave" of fibers in three orthogonal directions. In comparison to standard weaving methods, this process eliminates fiber crimp and forms a true 3D structure that can be tuned in tension, compression, and shear to match native cartilage properties. Most current 3D textile composite materials are constructed by laminating multiple 2D structures together; here, the use of a true 3D woven structure eliminates the weak interfaces between multiple layers in the structure, where delamination can occur. Furthermore, the controlled regularity and interconnectivity of the woven pore structure allow cells to be easily loaded and uniformly distributed within the scaffold upon which they are able to synthesize a robust extracellular matrix (Fig. 1) (*7*, *9*, *10*, *13*). The regular pore geometry also facilitates nutrient diffusion along regular and continuous paths throughout the scaffold (*7*). These properties have been optimized to mimic the functional properties of articular cartilage and have demonstrated their ability to sustain functional properties over extended in vitro culture (*7*, *9*, *10*, *13*). To enhance stable integration of the 3D woven textile into the bone bed, an additively manufactured porous base has also been integrated into the implant (Fig. 1, F and G). This type of structure has been shown in previous work to promote osteogenesis of transplanted stem cells by stimulating signaling pathways that enhance osteogenesis (*14*).

The objective of this work was therefore to test the ability of this bicomponent tissue-engineered construct to replace most of the

[1]Cytex Therapeutics Inc., Durham, NC, USA. [2]Translational Research in Pain Program, Department of Clinical Sciences, College of Veterinary Medicine, North Carolina State University, Raleigh, NC, USA. [3]Department of Clinical Sciences, College of Veterinary Medicine, North Carolina State University, Raleigh, NC, USA. [4]Medical College of Wisconsin, Milwaukee, WI, USA. [5]Department of Statistics, North Carolina State University, Raleigh, NC, USA. [6]Division of Bone and Mineral Diseases, Washington University School of Medicine in St. Louis, St. Louis, MO, USA. [7]Shriners Hospitals for Children—St. Louis, St. Louis, MO, USA. [8]Department of Pathology and Immunology, Washington University in St. Louis, St. Louis, MO, USA. [9]Department of Veterinary Clinical Sciences, College of Veterinary Medicine, Purdue University, West Lafayette, IN, USA. [10]Department of Orthopaedic Surgery, Washington University in St. Louis, St. Louis, MO, USA. [11]Center of Regenerative Medicine, Washington University in St. Louis, St. Louis, MO, USA. [12]Comparative Pain Research and Education Center, College of Veterinary Medicine, North Carolina State University, Raleigh, NC, USA. [13]Thurston Arthritis Center, UNC School of Medicine, Chapel Hill, NC, USA. [14]Center for Translational Pain Research, Department of Anesthesiology, Duke University, Durham, NC, USA.
*Corresponding author. Email: bradley.estes@cytextherapeutics.com (B.T.E.); guilak@wustl.edu (F.G.); dxlascel@ncsu.edu (B.D.X.L.)
†These authors contributed equally to this work as co–first authors.
‡These authors contributed equally to this work as co–senior authors.

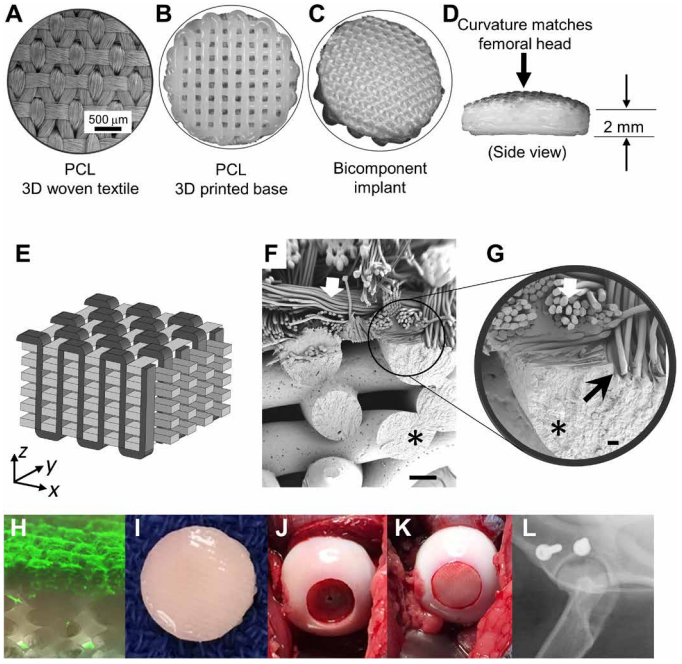

Fig. 1. Implant configuration and surgical procedure. (**A**) The cartilage component is constructed of a 3D woven textile, and (**B**) additive manufacturing is used to make a printed base, which, when fused together, form the (**C**) final bicomponent implant (**D**) 10 mm in diameter by ~2 mm deep. (**E**) 3D schematic of the woven textile demonstrating orthogonality of the structure. (**F** and **G**) Scanning electron microscopy images demonstrate bonding and encapsulation (black arrow) of woven yarns (white arrows) in the first layer of the printed PCL component (black asterisks). Scale bars, 100 μm. (**H**) MSC seeding (green fluorescence) is followed by (**I**) expansion, differentiation, and tissue development ex vivo. (**J**) Control defect site and (**K**) implant disposition are shown at the time of surgery. (**L**) A capsulorrhaphy procedure, standard in the canine model, was used to stabilize the joint. Photo credit: Franklin Moutos, Cytex Therapeutics Inc.

load-bearing cartilage surface of the femoral head in a large animal model, using autologous bone marrow–derived mesenchymal stem cells (MSCs) on an anatomically shaped 3D woven scaffold (*7*, *10*, *11*). Our hypothesis was that a scaffold engineered to mimic many of the mechanical properties of the native tissue with sufficient porosity for cell ingrowth and tissue differentiation (*7*–*9*, *11*) could restore the articular surface structure and, thereby, also restore normal function to the joint. To test this hypothesis, we used a canine model of hip OA, because of its similarities in the human hip, and collected quantitative functional outcome data longitudinally throughout the 6-month duration of the study (*15*–*17*). The bicomponent nature of the 3D woven textile and additively manufactured base enable a novel treatment paradigm for osteochondral repair for large lesions that cannot be repaired with current bone marrow stimulation techniques.

RESULTS

Outcome measures in this study were primarily focused on behavioral measures of joint pain and function (i.e., gait analysis), with concomitant analysis of the structural integrity and mechanical properties of the regenerated tissues at the 6-month termination of the study.

Gait analysis, limb girth, pain, and actimetry

The implant group trended toward baseline in all gait analysis measures and was also found to return to baseline in three of the five measures (Fig. 2). For peak vertical force (PVF), which is one of the principal components for quantifying lameness, the implant group indicated better limb use, quantified as 6.82 ± 2.23% body weight (BW) larger than the control group's average across all time points (Fig. 2A). The animals receiving the implant returned to baseline PVF by month 3. For vertical impulse (VI), another principal measure for quantifying lameness, the implant group returned to normal by the sixth month, and over the 6-month period, the implant average was 0.67 ± 0.19% BW·s larger than the control group animals, also indicating better limb use (Fig. 2B). Both implant and control groups did not return to baseline for peak propulsion force (PPF) and propulsion impulse (PI), but it was noted that the implant group was trending toward baseline faster than the control group for both measures (Fig. 2, C and D). Although body weight distribution returned to baseline for both implant and control groups, that return happened 1 month earlier for the implant group than it did for the control group (Fig. 2E). Along with the gait analysis measures, the discrepancy in limb girth between operated and unoperated contralateral limb trended toward normal at a faster rate in the implant group than the control group, but neither group returned to baseline over the duration of the study (Fig. 2F). This finding was confirmed by computed tomography (CT) analysis at the end of the study when comparing the cross-sectional area of the thigh of the experimental limb to the contralateral, unoperated limb. The control animals had a −15.3 ± 8.1 cm^2 difference (operated minus unoperated) in area, and the implant animals had a −5.3 ± 4.3 cm^2 difference in area. For pain, as measured by the Canine Research Orthopedic Pain Inventory (CROPI-h; see also fig. S1), the implant group's score was 6.82 ± 2.23 smaller (less pain and impairment) than the control group's average across all time periods, and the dogs receiving the implant returned to normal preoperative levels of pain and function by the second month of the study (Fig. 2G and fig. S1). Body weight for all animals within each group was consistent throughout the study period (Fig. 2H).

Overall, the (negative) effect on activity was greater in the control group than implant group (Fig. 3), with the implant group regaining baseline activity by the end of the first postoperative month when examining peak hours of activity (Table 1). Significant treatment effects were observed at each monthly interval ($P = 0.0031$). Significant interactive effects were also noted, particularly month*hour ($P < 0.05$) and treatment*hour ($P < 0.0001$) as observed by the different trends in the two peaks of activity measured when the animals were interacting with the care technicians. Averaged across the 6-month period, significant differences were noted between the hours of 7:00 a.m. and 4:00 p.m.

Variables of time (i.e., month of analysis) and treatment (control versus implant) were significant for measured values of gait analysis, limb girth, and CROPI-h (Table 1); however, no time/treatment interactive effects were observed in the study. A treatment effect was insignificant in only two of the nine measures: static body weight distribution and OA radiographic score.

Radiographic scores of OA and synovium histology; organ pathology

Ventral-dorsal radiography demonstrated no noticeable issues in the implant group, although bone loss and exostosis in ring form were

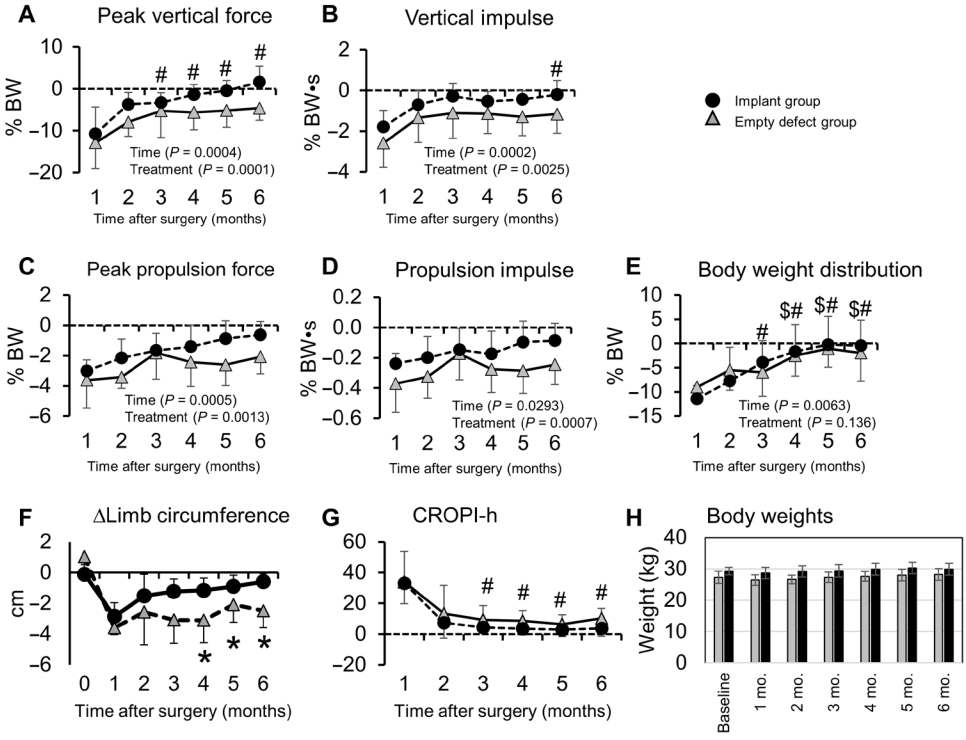

Fig. 2. Gait analysis. Measured kinetic GRF indices including (**A**) PVF, (**B**) VI, (**C**) PPF, and (**D**) PI (all based on % BW) rapidly returned to baseline in the implant group; conversely, the empty defect group kinetic indices never returned to normal. (**E**) Body weight distribution of the operated limb in standing (measured by a pressure-sensitive walkway) showed a return to baseline in both groups. Data are presented as change from baseline, normalized by BW. (**F**) Change in limb circumference as measured by the difference between operated limb and contralateral unoperated limb indicates recovery of muscle volume in the implant group and persistent atrophy in the empty defect group, $^*P < 0.05$. (**G**) Pain scores (CROPI-h) were consistently lower in the implant group compared to the control group; however, no time/treatment interaction was observed ($P = 0.075$). (**H**) Weights of animals throughout the study. Means ± SD with a two-factor (treatment and time) ANCOVA model were used with responses d_{ijk} and covariate x_{ij}: Overall time and treatment effect P values are noted on figures, no time*treatment interactive effects were observed in any of the measures. # indicates no difference from baseline in the implant group; $ indicates no difference from baseline in the control group, $P < 0.05$.

evident in the control group (Fig. 4A). OA radiographic scoring indicated normal joint findings for the implant group in months 1 and 2, while significant differences were noted between preoperative values and postoperative radiographic markers for all time points following surgery in the control animals (Fig. 4, B and C). Mild synovitis was observed on all operated hip joints (Fig. 4, D and E). While no significant differences were noted between control and implant synovium, trends of higher chronic inflammation and synovial hyperplasia, along with more giant cells, were observed in the untreated joints than in the implant joints (Fig. 4F). Heart, kidney, spleen, lung, liver, and skeletal muscle all showed no aberrant pathology, including inflammation. Regional lymph nodes showed mild reactive changes, including scattered giant cells that were likely related to the surgical procedure, as they were similar in control and implant groups.

Cartilage and subchondral bone: Gross and histological findings, immunohistological findings, and day 0 biochemical findings

No depressions were observed in the implant-treated femoral heads (Fig. 5, A to C), and the surface of the implant appeared to be smooth with no surface irregularities. In contrast, control defects showed depressions into the osteochondral bone (Fig. 5, D to F) with only fibrous connective tissues in the osteochondral defects (Fig. 5G). Cartilaginous tissue ingrowth and overgrowth occurred both in and on the woven phase of the bicomponent device (Fig. 5, H and I), and a consistent finding was that these tissues appeared to be bonded to adjacent cartilage at the periphery of the device with no fissures at either end of the device (Fig. 5, J and K). In addition, a limited amount of bone integrated with the printed portion of the implant was observed with no fissures between the implant and the surrounding bone (Fig. 5, I and M). Tissue filling the pores between the poly(ε-caprolactone) (PCL) printed struts consisted primarily of fibrous tissue (Fig. 5L). Microradiographs showed no reduction in bone mineral density adjacent to the implant and minimal ingrowth into the textile component of the implant (Fig. 5M). Typical cross sections of the implant demonstrated fibrous overgrowth, complete tissue infilling of the pores in both components of the implant (i.e., both textile and printed portions) with the implant intact at this 6-month terminal time point (Fig. 5N). Rounded chondrocyte-like cell morphology within the pore structure of the textile was also observed (Fig. 5O). There was no inflammation observed in peri-implant tissues. In addition, there were no changes in the histological sections of the acetabula in either the control or implant hips. Immunohistochemical labeling for collagen types I and II revealed fibrous structure in the textile component alone containing both collagens at the time of implantation (Fig. 6). The empty defect control group was completely filled with type I collagen only, while the

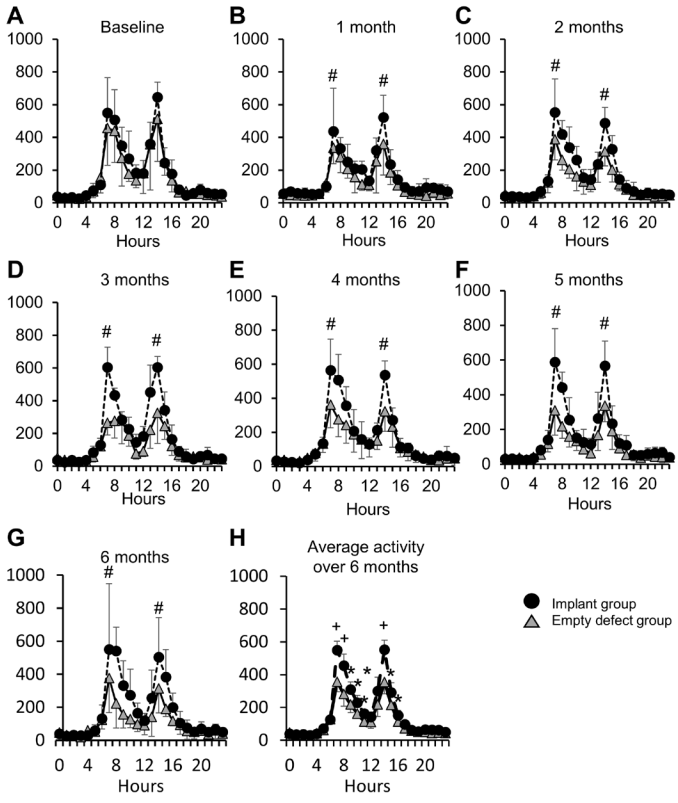

Fig. 3. Actimetry data. (**A** to **H**) Total activity count expressed as the average per minute activity over the preceding 2-week period, shown for each hour of the day (at baseline, 1, 2, 3, 4, 5, and 6 months postoperatively). Significant treatment effects were observed at each monthly interval ($P = 0.0031$). Significant interactive effects were also noted, particularly month*hour ($P < 0.05$) and treatment*hour ($P < 0.0001$) as observed by the different trends in the two peaks of activity measured when the animals were interacting with the care technicians. (H) Across the 6-month period, significant differences were noted between the hours of 7:00 a.m. and 4:00 p.m. (*$P < 0.05$ and +$P < 0.0001$). The implant group returned to baseline at hours 7 and 14 in month 1, while the control group never returned to baseline. # indicates no difference from baseline in the implant group at hours 7 and 14.

implant contained a mixture of both type I and II collagen at the 6-month time point. These collagens were found colocalized in both the textile and printed components of the implants (Fig. 6). Dimethylmethylene blue normalized to double-stranded DNA (dsDNA) and hydroxyproline (OHP) normalized to dsDNA revealed sulfated glycosaminoglycan (sGAG)/DNA at 12.39 μg/μg and total collagen/DNA of 102.1 μg/μg for day 0 constructs (*18*).

Modified O'Driscoll scores showed that the control group had the greatest reduction in histology scores, whereas the implant group had significantly higher scores, indicating histology closer to baseline than untreated defects (Fig. 7). Eleven of the 12 unoperated normal (i.e., contralateral) femoral heads had a histology score of 20/20 and was 18/20 in the other. The range for the control defects was 6 to 9 and 13 to 14 for the implants. There was a significant difference between the two groups ($P = 0.0001$) for the operated to unoperated difference in histology score. The average difference in the control group was −13.0 ± 0.63 (SEM), and in the implant group, it was −6.8 ± 0.17. In comparing the implant to the unoperated cartilage control, the implant was not significantly different in five of the eight components of this scoring rubric, which included surface irregularity, cartilage level, adjacent cartilage bonding, presence of inflammatory cells, and chondrocyte clustering. The measures that were significantly different were subchondral bone regeneration, freedom from adjacent tissue degeneration, and hyalinity (Fig. 7).

Mechanical properties

At the time of implantation, the implants had a mean compressive instantaneous modulus of 5.93 MPa with a mean compressive equilibrium modulus of 4.61 MPa. After 6 months in vivo with significant tissue both in and on top of the surface of the implants, both the instantaneous and equilibrium moduli of the implant were significantly decreased from day 0 values to 0.99 and 0.46 MPa, respectively. Significant differences were observed in the mechanical properties of the implant repair tissue as compared to control tissue, with a greater than 10-fold higher modulus in the implant group (equilibrium modulus: 0.460 MPa versus 0.039 MPa for the implant and control groups, respectively; instantaneous modulus: 0.99 MPa versus 0.293 MPa for the implant and control groups, respectively) ($P < 0.05$). The instantaneous modulus of the contralateral control (unoperated) was approximately 4-fold higher than the repair tissue with the implant group but was 15-fold higher than the instantaneous modulus measured in the empty defect repair tissues ($P < 0.0001$). The equilibrium modulus of the contralateral control cartilage was more than 2-fold greater than the repair tissue in the implant group ($P < 0.05$) but was more than 30-fold higher relative to the empty defect repair tissue ($P < 0.0001$) (Fig. 8).

DISCUSSION

The findings of this study show that an anatomically shaped tissue-engineered implant consisting of an interconnected 3D woven and 3D printed composite can provide functional restoration of massive osteochondral defects in the hip joint. Excellent integration of this MSC-seeded construct was observed in all cases, and no failures were observed. Pain and function outcomes in the animals receiving the construct showed significant improvement by the first measured time point (1 month) and demonstrated a return to normal preoperative values by the 6-month time period. The implants showed mechanical properties approaching those of normal cartilage, as compared to unfilled defects, which showed a compressive modulus of less than 10% that of implant tissues.

The primary objective measures used in this study were derived from biomechanical analysis to determine the functional response of joint restoration following the creation of a massive (10 mm) defect in the hip. This massive defect comprised approximately 60% of the major load-bearing surface of the femoral head and is much larger than what is typically observed in clinical practice. In context, the created lesion was approximately twice the size of early clinical lesions in this area that are associated with clinical signs of OA in dogs. An empty defect alone served as a control for the implant group since, clinically, the size of the lesion would not spontaneously heal and would also progressively lead to joint degeneration. In addition, the bone preparation used was effectively a bone marrow stimulation technique that is analogous to techniques that are currently used clinically, such as microfracture. Gait analysis has been validated as an objective measure of changes in limb use as it relates to joint pain in dogs and humans (*19*, *20*). The decrease in kinetic ground reaction forces (GRFs) from baseline to 6 months following surgery in the control group was similar to the difference between that in

Table 1. Summary of statistical findings relative to baseline. "Control," control group; "Implant," implant group.

Measure	Time (month)	Treatment	Time* treatment	First month control avg. – baseline avg.	First month implant avg. – baseline avg.	Sixth month control avg. – baseline avg.	Sixth month implant avg. – baseline avg.	Control return to baseline (month)	Implant return to baseline (month)
Peak vertical force	$P < 0.0005$	$P < 0.0005$	$P > 0.05$	−14.15 ± 1.54	−9.39 ± 1.54	−3.86 ± 1.05	0.91 ± 1.05	–	3
Vertical impulse	$P < 0.005$	$P < 0.005$	$P > 0.05$	−2.52 ± 0.25	−1.85 ± 0.25	−1.02 ± 0.18	−0.35 ± 0.18	–	6
Peak propulsion force	$P < 0.005$	$P < 0.005$	$P > 0.05$	−3.80 ± 0.31	−2.82 ± 0.31	−1.84 ± 0.27	−0.86 ± 0.27	–	–
Propulsion impulse	$P < 0.05$	$P < 0.05$	$P > 0.05$	−0.36 ± 0.03	−0.25 ± 0.03	−0.23 ± 0.03	−0.11 ± 0.03	–	–
Static body weight distribution	$P = 0.0063$	$P > 0.05$	$P > 0.05$	−11.50 ± 2.12	−8.89 ± 2.12	−2.50 ± 1.13	0.11 ± 1.13	3	3
Activity at 7:00 a.m.*	$P < 0.05$	$P < 0.05$	$P > 0.05$	−196.54 ± 47.97	−20.03 ± 49.34	−118.69 ± 47.93	47.13 ± 49.28	–	1
Activity at 2:00 p.m.*	$P < 0.05$	$P < 0.05$	$P > 0.05$	−220.52 ± 39.79	−41.19 ± 40.99	−249.49 ± 39.73	−80.86 ± 40.93	–	1
CROPI-h	$P < 0.05$	$P < 0.05$	$P > 0.05$	36.82 ± 5.89	30.01 ± 5.89	10.24 ± 1.88	3.43 ± 1.88	–	2
Limb girth	$P < 0.005$	$P < 0.005$	$P > 0.05$	−4.59 ± 0.37	−3.00 ± 0.37	−2.85 ± 0.34	−1.25 ± 0.34	–	–
OA radiographic score	$P = 0.0089$	$P > 0.05$	$P > 0.05$	2.59 ± 0.96	1.41 ± 0.96	4.67 ± 0.77	3.49 ± 0.77	–	1 and 2

*Additional time/hour interaction for the actimetry data, $P = 0.036$.

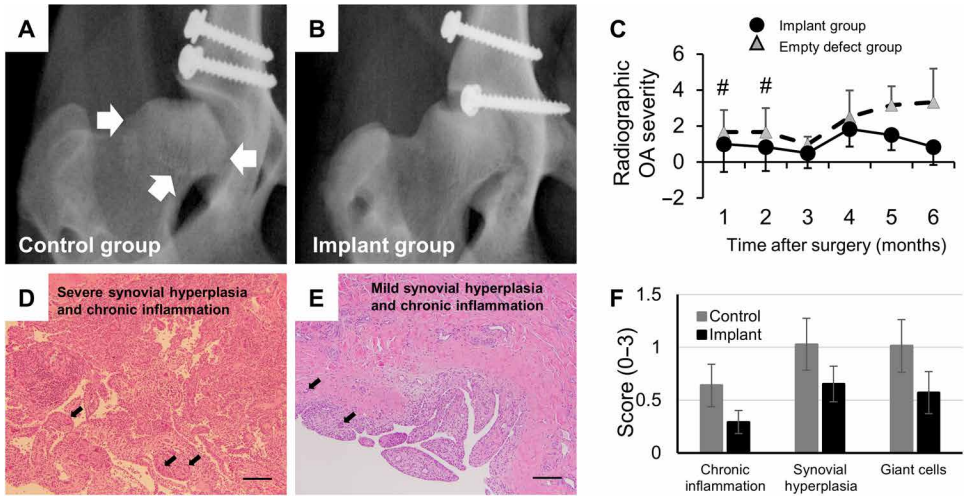

Fig. 4. Radiographic and synovial inflammation suggests inhibition of OA progression in the treatment group. Ventral-dorsal radiographic examples demonstrate (**A**) obvious bone loss and exostosis in ring form (white arrows), giving a slight conical appearance of the femoral head in the control animals and (**B**) what appears to be a radiographically healthy joint in the experimental implant group as noted by the absence of any extraarticular bone remodeling. (**C**) Radiographic OA severity shows a significant effect of time ($P = 0.0005$) but not treatment, although a trend was noted toward a treatment effect at the later time points ($P > 0.05$; # indicates no difference from baseline in the implant group). Histological sections showing (**D**) severe and (**E**) mild cases of synovial hyperplasia and chronic inflammation, respectively, with black arrows indicating examples of giant cells. H&E histology stain: Scale bars, 0.1 mm. (**F**) Semiquantitative scoring of synovial tissues (maximum score of 3: normal, 0; mild, 1; moderate, 2; and severe, 3) for chronic inflammation severity, synovial hyperplasia severity, and the presence of giant cells. Further details of the scoring matrix are provided in table S1.

clinically sound dogs and dogs with naturally occurring hip OA, as well as that in humans between patients with OA and non-OA patients (*21*). Furthermore, the return toward normal GRFs by 3 to 6 months following the surgery in the implant group was similar to the changes following successful total hip replacement (THR) in dogs (*19*, *22*). Seibert and colleagues (*22*) reported PVF and VI of pet dogs with diagnosed OA and undergoing THR. On average, the animals with naturally occurring OA had PVF deficits of 7.5% BW relative the contralateral limb, similar to the difference between the operated and control limbs of the control group (empty defect) dogs (~5% BW). THR in pet dogs resulted in a 3.65% BW improvement in limb use (with up to 12 months of follow-up), and in our study, the difference in PVF between the control and seeded group was ~11% BW at 6 months. Similarly, VI of the operated limb in pet dogs was increased approximately 1% after hip replacement, also in line with the difference between control and seeded scaffold groups at 6 months (1%) (*22*). Together, GRF data obtained in the current study suggest equivalent or greater functional outcomes to that which is obtained with total hip arthroplasty, which is validating for our approach. It is well established that a THR alleviates pain and lameness in the canine hip (*23*), and the fact that we obtained equivalent changes in both PVF and VI strongly suggests palliation of pain and lameness, which was also confirmed across our measures in the present study. Although there were no significant differences between groups, an analysis of body weight distribution to the operated limb at 6 months following surgery in the implant group was closer to baseline than the control (empty defect) group. The increase in the body weight distribution of ~10% over the 6-month study in the implant group over time is completely consistent with what was observed in a previous study for dogs with a unilateral THR in dogs (*17*) and in humans that had undergone unilateral total hip arthroplasty (*24*). Overall, dynamic and static GRFs suggest that our biological resurfacing technique restores limb function following surgery.

Additional measures of the efficacy of this procedure were made using activity measurement with accelerometers, which provide a validated surrogate measure of movement as a measure of pain and function (*25*) and have successfully been used to detect changes in activity related to analgesic therapies in clinical OA studies in dogs (*26*). In the present study, we observed significant reductions in activity in the control (empty defect) group, indicative of ongoing pain and functional deficits that persisted throughout the 6-month study period. However, in the implant group, no significant differences between baseline and overall postoperative activity levels were observed, indicating an absence of pain. In terms of patterns of activity, we observed a bimodal pattern, similar to that that has been described in research in pet dogs (*25*, *26*). The peaks of activity were primarily affected in the present study in the control (empty defect) dogs, and these peaks represent more intense activity. The provision of effective analgesia (anti–nerve growth factor monoclonal antibody) in pet dogs similarly affected these peaks of activity (*26*). These measurements are consistent with the patterns of reduced activity observed in humans with OA compared to healthy humans (*27*).

The change from baseline in limb girth, as calculated by the difference between operated and unoperated contralateral limb, mirrored the change from baseline in limb use. In the implant group, limb circumference increased as kinetic variables returned to preoperative values, whereas the control group's limb circumference never returned to the baseline, matching the reduced limb use. This relationship between limb use and muscle mass is similar to what is seen in humans (*28*). The limb girth measurements were supported by the objective measurement of thigh muscle cross-sectional area using CT, and there was a significant correlation between these two measures ($r = 0.58$, $P = 0.0063$) at the 6-month time point.

A critical design parameter of the tissue-engineered implant was the ability to reproduce the mechanical properties and anatomic structure of the cartilage defect from the initial time of implantation.

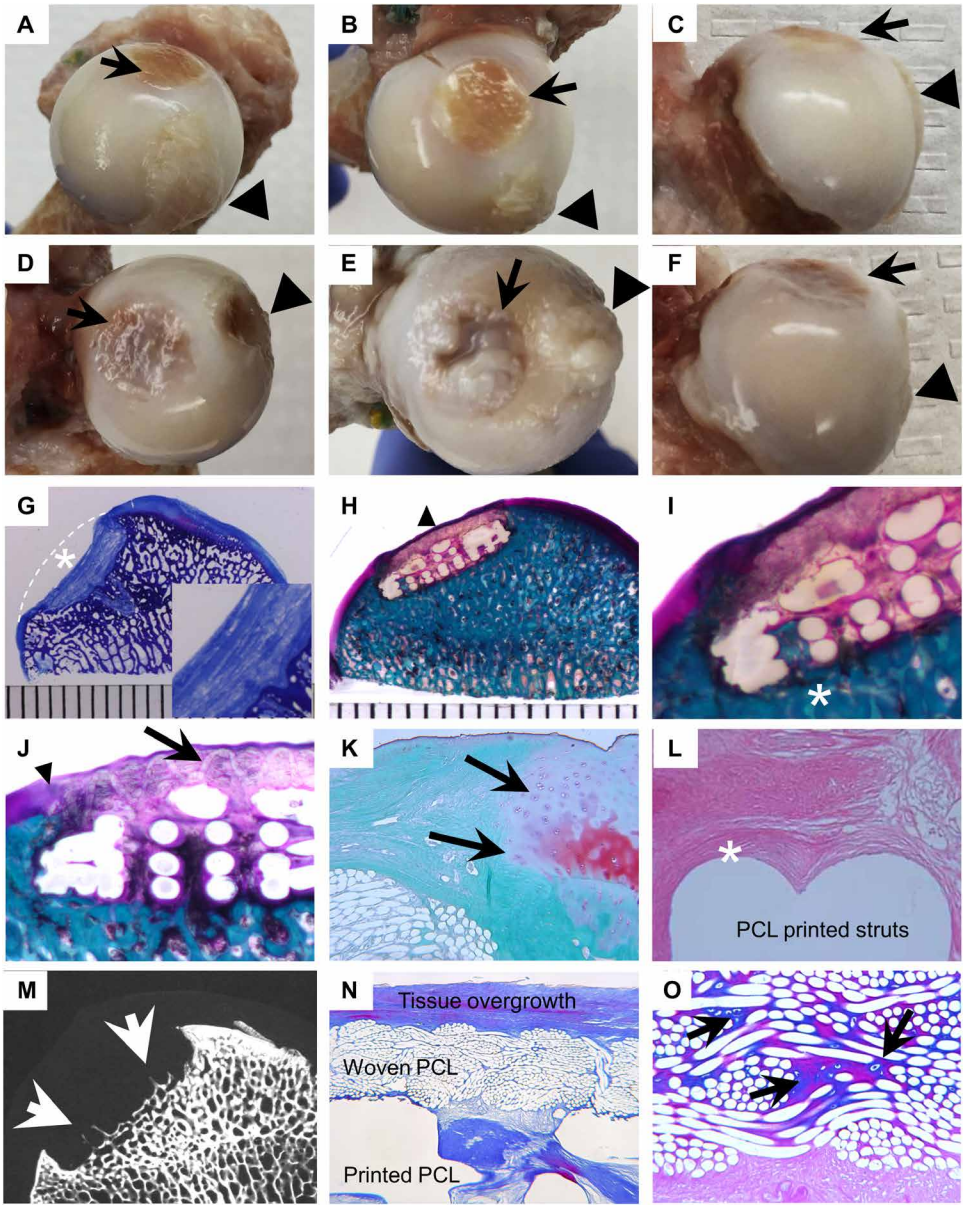

Fig. 5. Gross findings/histology. (**A** to **C**) The smooth implant contour typically matched native anatomy (dog 6) (black arrows). Round ligament is visible (black arrowheads). (**D** to **F**) Empty defects (left to right: dogs 7, 2, and 7) (black arrows) showed significant fibrocartilage filling. (**G**) Mallory Aniline Blue (MAB) of empty defects (dog 13) showed unhealed fibrous-filled depressions (white asterisk – dotted line = ~original articular surface). Inset (millimeter scale): Magnification of defect. (**H**) Undecalcified implant section (dog 6) revealed host tissue integration and a smooth surface without irregularities (black triangle). Trichrome (millimeter scale) (**I**) with limited new bone formation (white asterisk). (**J**) Undecalcified section (dog 11) (trichrome) demonstrates congruency with native surfaces (black arrowhead). Z-fiber (black arrow) presence demonstrates implant integrity. (**K**) Representative Safranin O/Fast Green staining (dog 12) showed fibrous bonding to adjacent cartilage at defect margins (black arrows) (79×). (**L**) H&E (dog 11) showing fibrous tissue (white asterisk) around PCL struts (79×). (**M**) Representative microradiograph (dog 11) revealed limited bone formation within the base (white arrows). (**N**) Decalcified histology (dog 6) showed fibrous growth in/on the implant (MAB, 31×) (**O**) and few chondrocytes (dog 10) in the implant woven component (black arrows) (Alcian blue–periodic acid–Schiff, 79×). See figs. S2 to S8 and table S2 for all animal images. Photo credit: Bradley Estes, Cytex Therapeutics Inc.

These properties were conferred by the 3D orthogonal weaving method that was "tuned" to match the implant properties a priori (*9*, *11*). Tissue development in the implant served to significantly decrease the modulus values relative to day 0, revealing the contribution of the newly synthesized and remodeled tissue on the mechanical behavior of the biosynthetic composite. Regardless of the relative mechanical contribution of the PCL-based bicomponent implant and the newly synthesized tissues, our results confirm the restoration of the native anatomical contours with a hybrid biologic/synthetic implant that exhibited native cartilage compressive values. During the culture of the constructs, we only observed filling of the textile component with small amounts of de novo tissue (Fig. 6), but no tissue was synthesized in the printed component. Accordingly, all tissue that is observed in the printed base was synthesized in vivo

over the 6-month period. The fact that the initial printed base was devoid of cells and tissue at day 0 could account for why little bone development had occurred in the printed component of the implant, and perhaps, future studies using longer survival times may allow for this bone tissue development. Immunohistochemical labeling for type I and II collagen revealed only type I collagen in the empty defects, whereas colocalization of collagen types I and II is present in the implant group. These data suggest that the PCL implant is inducing (or, at a minimum, is conducive to) a more cartilage-like phenotype due to the production of type II collagen. The integration of this structure with native tissues allowed a seamless transition from native, preexisting tissue to de novo tissue, such that the joint could articulate freely in seemingly a pain-free state as confirmed by actimetry, gait analysis, limb girth, and pain assessment. Moreover, the mechanical properties also indicate values in the range of normal articular cartilage, underscoring the functionality of the tissues in the implant group at the 6-month time point. In total, these histological and mechanical analyses strongly supported our hypothesis that a tissue-engineered anatomically shaped implant could restore structure and functional properties of the tissue and then, as a consequence, that of the joint.

From a regulatory perspective, the implant used in this study would require a Biological License Application as a combination product regulated by both the Center for Biologics Evaluation and Research and the Center for Devices and Radiologic Health. The work presented here serves as preliminary data, providing early efficacy data on the approach with the bicomponent implant. Longer time points and other preclinical work would be required before entering phase 1 clinical trials.

Despite being the standard of care in hip OA, total joint replacement is not an ideal procedure for the young human patient population presenting with hip degeneration because they would likely require multiple revision surgeries in their lifetime, each iteration posing additional complications, quicker implant failures, and overall decreased satisfaction. Hence, there is a critical need for new interventions that delay or halt the progression of OA and the need for initial joint replacement. The approach for using such a construct as presented in this manuscript would be to stave off a traditional total hip arthroplasty procedure by providing pain relief and restoring an active lifestyle in this young and active human patient population. An important advantage of the method proposed is that the bioartificial implant is expected to integrate with the native bone while preserving the integrity of the bony structure of the joint. If, over time, disease progresses to the point that total joint replacement is an appropriate choice of treatment, then the joint could be readily converted to a standard joint replacement procedure. Because little or no bone is

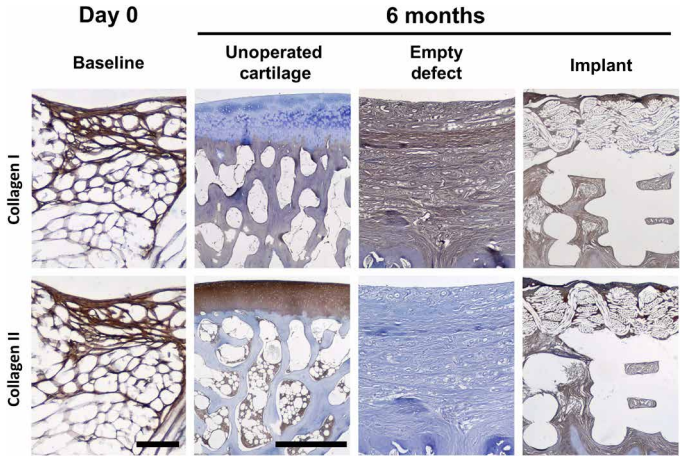

Fig. 6. Immunohistochemical labeling for collagen I and II at day 0 and after 6 months in vivo. Scale bars, (day 0 implants) 0.1 mm and (6-month tissues/implants) 1 mm. Day 0 specimens are both from dog 12. Unoperated cartilage images are from the left femoral head of dog 13. Empty defect images are from the right femoral head of dog 13, and the implant images are from dog 11.

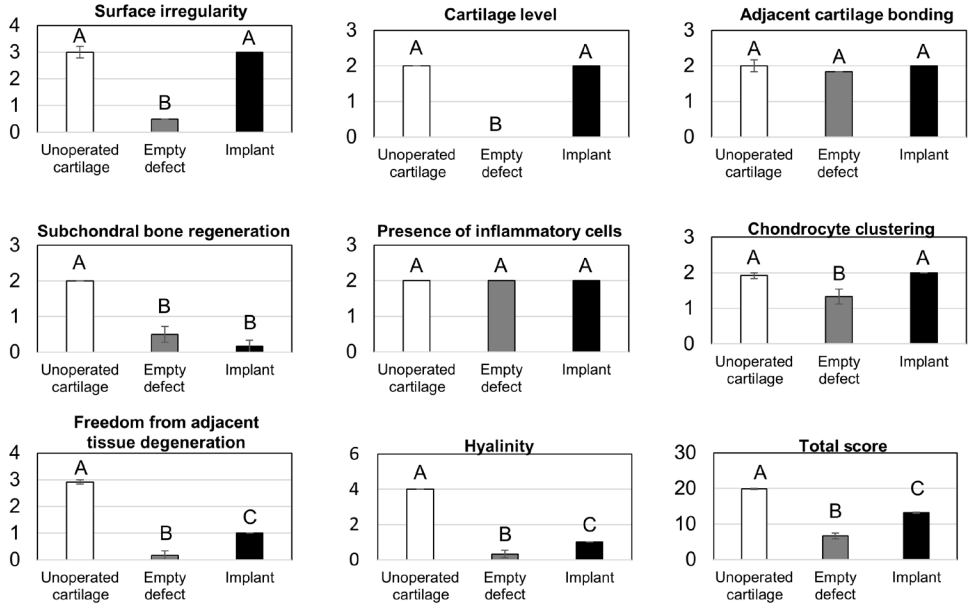

Fig. 7. Modified O'Driscoll scoring per component and total score. Higher scores indicate better healing. Maximum score is 20 points. Groups not sharing the same letter are statistically different (Student's *t* test for comparisons of each pair, $P < 0.05$).

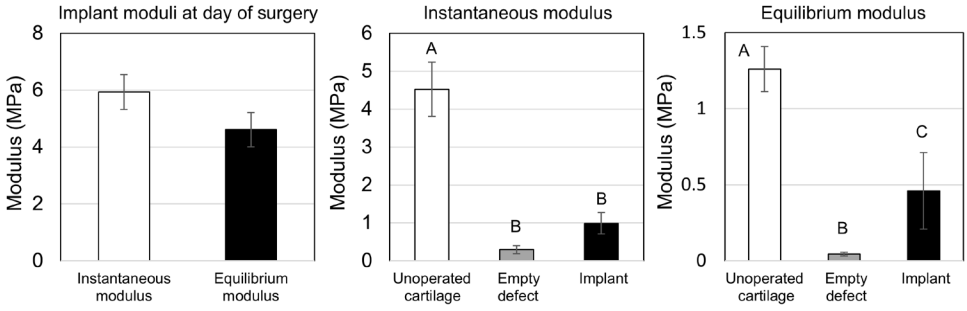

Fig. 8. Instantaneous and equilibrium compressive moduli of implants at day of surgery and after 6 months in vivo. Groups not sharing the same letter are statistically different [analysis of variance (ANOVA), $P < 0.05$].

removed in the initial implantation of the implant, native bone is preserved for resurfacing arthroplasty or total hip arthroplasty procedures. Consequently, there would be few potential drawbacks as compared to an initial joint replacement surgery. Furthermore, because the components of the implant are bioresorbable, the risk of adverse events due to small wear products is greatly reduced. Regarding resorption, the choice of PCL was also deliberate, given its long resorptive profile in vivo on the order of years, the bioinert nature of the material, and the lack of acidic by-products as it breaks down (*29*, *30*). Our expectation, given these characteristics, is that the newly synthesized tissue will continue to remodel as more percentage of the load is borne by the newly synthesized tissue as the PCL resorbs. Longer preclinical studies and, perhaps, even clinical trials will be required to fully assess the resorptive nature and functionality of this tissue over time.

In summary, all functional outcome metrics including activity measurement, dynamic and static gait/standing analysis, and radiographic monitoring demonstrated that the animals receiving the implant returned to normal preoperative values by the 6-month time period. These functional outcome measures are all highly relevant to human patients. Furthermore, the osteochondral defect was placed in a clinically relevant, load-bearing position, indicating that the implant was able to effectively restore the functional capacity of the joint at early times. Although the phenotype of the repair tissue is not fully characterized, the data from histology, immunohistochemical, and mechanical analyses, in combination, confirm the structural integrity of the implant, its integration with surrounding tissues, and the restoration of the articular surface, thereby providing a basis and explanation for the functional outcomes that we observed in this study. On the basis of the clinically relevant outcome measures that were investigated, our data provide evidence that a textile-based, anatomically shaped resorbable construct can be combined with MSCs for a potential therapy for the treatment of early- to moderate-stage OA.

MATERIALS AND METHODS

Animals

All animal procedures were approved by the North Carolina State University Institutional Animal Care and Use Committee (#13-010-B). Purpose-bred sexually intact male hound dogs ($n = 16$, 25 to 31 kg) were purchased at 2 years of age from an approved vendor. Dogs were assigned to a study group if deemed healthy and free of clinical orthopedic disease based on clinical examination by a board-certified orthopedic surgeon veterinarian, complete blood count, blood chemistry, and urinalysis. Bloodwork and urinalysis were also performed before termination. Dogs were sedated and radiographed to evaluate for preexisting hip dysplasia, radiographic OA, and closure of the proximal femoral growth plates. Following the initial evaluation, 12 dogs were randomly allocated to either control group (control; $n = 6$) or tissue-engineered scaffold implant group (implant; $n = 6$). The remaining dogs ($n = 4$) were adopted out because of preexisting hip OA and/or behavior incompatibility with study requirements. All allocated dogs underwent hip surgery on one side, and the contralateral hip was used as the normal control. Surgery was performed on the coxofemoral joint with the least OA and associated signs based on clinical assessment and radiography.

Dogs were housed in climate-controlled individual housing with room temperature and humidity maintained at 23°C and 30 to 70%, respectively. Rooms were on a 12:12 light:dark cycle (light time: 6:30 a.m. to 6:30 p.m.), with rotating enrichment toys and features. The dogs were allowed to move freely inside their runs but were acclimated for 2 months before surgery to lowered ceilings to prevent jumping up. The bedding area was placed on the floor with a step-up of only 7.6 cm. The dogs were fed according to their caloric needs and allowed ad libitum access to water during the study. The dogs were walked on leash for 10 min a day until surgery for socialization, training to the leash, and enrichment. The dogs were transported to the data collection room for 20 to 30 min/day for acclimation to performance activities involving the study equipment (e.g., trotting across the force plate and standing on the pressure-sensitive walkway).

Perioperative management

Preemptive analgesia was provided by a fentanyl patch (75 or 100 μg, depending on dog weight) applied to the body wall. Dogs were premedicated with acepromazine (0.025 mg/kg, sc) and midazolam (0.2 mg/kg, sc). An intravenous catheter was placed, and propofol was administered to effect to induce general anesthesia. Anesthesia was maintained using isoflurane carried in oxygen and delivered via an endotracheal tube and circle circuit. Dogs ventilated spontaneously. Vital signs were monitored with electrocardiography, pulse oximeter, blood pressure (oscillometry), and capnography throughout anesthesia and recovery. Epidural bupivacaine (0.5 mg/kg) and preservative-free morphine (0.1 mg/kg) were administered preoperatively. Prophylactic antibiotics (cefazolin; 22 mg/kg, iv) were given at least 15 min before surgery and then every 90 min during surgery. Immediately after surgery, an adhesive bandage and Ioban (3M, St. Paul, MN) were applied to the surgical wound and replaced as needed until the wound was healed (approximately 5 to 7 days).

Acetaminophen (15 mg/kg, q12h) and gabapentin (10 mg/kg, q12h, given orally) were administered postoperatively for 21 days. Additional analgesia (0.1 to 0.2 mg/kg, sc, of meloxicam or 4.4 mg/kg of carprofen orally) was provided if pain was detected on examination (M.E. and B.D.X.L.) at any time.

Bone marrow aspiration

Dogs assigned to the implant group had bone marrow aspirated under general anesthesia 6 to 8 weeks before surgery. Following aseptic preparation of the area, bone marrow was collected from the proximal humerus using an 11G Jamshidi biopsy needle, and 10 to 15 ml of bone marrow were collected into a syringe containing 2000 U of heparin. Bupivacaine was injected locally following the procedure, and carprofen was administered for a total of 3 days following the procedure. Bone marrow was immediately transported on ice to the laboratory for subsequent cell cultures.

Tissue-engineered implant

The implant (Fig. 1, A to D) consisted of a novel bicomponent structure that combined a biomimetic 3D woven textile (Fig. 1A) for reconstructing the cartilage layer with a porous 3D printed structure, previously shown to have osteoconductive properties (*31*). Multifilament resorbable PCL yarns (EMS-GRILTECH, Domat, Switzerland) measuring ~150 μm in diameter were woven in three orthogonal directions (*x*, *y*, and *z* directions) using 48 *x*-direction yarns/cm, 75 *y*-direction yarns/cm, and 12 *z*-direction yarns/cm, resulting in an overall porosity of 52.5%. A schematic of the structure is depicted in Fig. 1E. The 3D osteoconductive base (Fig. 1B) was manufactured by direct extrusion (500 ± 50 μm) using a 3D printer (EnvisionTEC 3D-Bioplotter). The textile and printed phases were bonded using localized heat under microscopic guidance to integrate the structures. More specifically, by taking advantage of the ability of PCL to retain heat, the top layer of the additively manufactured base was heated to ~65°C, and then the textile is pressed into place to incorporate the layers under stereomicroscopic guidance. The resulting interface can be seen in Fig. 1 (F and G). Both phases of the implant were made using PCL of molecular weight 50 to 60 kDa. The bicomponent woven/printed PCL scaffolds were immersed in a 4 M NaOH bath for 15 to 16 hours to clean the fibers and increase their surface hydrophilicity.

Cell culture and seeding of scaffold

Collected bone marrow from the initial 10 to 15 ml of aspirate was divided between two 50-ml centrifuge tubes, and phosphate-buffered saline (PBS) was added to a total of 45 ml of volume per tube. Samples were centrifuged for 15 min at 300*g* to create a pellet of cells. The supernatant was aspirated, PBS was added, and the procedure was repeated an additional three times until a loose, but clearly identifiable, pellet was obtained on the fourth PBS wash. The cell pellets were resuspended in 30 ml of MSC expansion media—consisting of Dulbecco's modified Eagle's medium (DMEM); 10% fetal bovine serum; penicillin, streptomycin, and fungizone (P/S/F); and basic fibroblast growth factor (1 ng/ml)—and were divided equally among three T225 flasks. Expansion media (20 ml) was added to each flask to give a final volume of 30 ml per flask. A complete medium exchange occurred after 24 hours and then three times per week until cells were removed for implant seeding after 1 week. The cells were removed using 0.05% trypsin EDTA (5 ml per flask) and incubated at 37°C, 5% CO_2 for 3 to 5 min. Cells were harvested into 10 ml of expansion media and pelleted at 200*g* for 5 min. The pellet was aspirated and resuspended at a concentration of 20 million cells/ml of MSC expansion media. Cells were seeded in a 25-μl volume to the textile surface of the implant, and the scaffolds were placed in the incubator (37°C, 5% CO_2) and allowed to attach to the 3D woven structure for 1 hour, after which the scaffolds were turned upside down and 1 ml of media was added to each scaffold. After 2 days, another 1 ml of expansion medium was added to the cultures and cultured for another 14 days. The cell-seeded implants were subjected to complete media exchanges three times per week irrespective of medium. After 14 days in expansion medium, the cultures were switched to chondrogenic medium consisting of DMEM-HG, ascorbic acid (37.5 μg/ml), 100 nM dexamethasone, 1× P/S, 1× insulin/transferrin/selenic acid (ITS+), and transforming growth factor–β3 (10 ng/ml) for an additional 28 days before implantation.

Surgery

A standard craniolateral approach to the selected coxofemoral joint was performed. Following round ligament transection and joint dislocation, a 1.1-mm diamond-tip K-wire was inserted into the femoral head (midpoint between the round ligament and lateral edge of the femoral head), perpendicular to the surface in all directions, and to a depth of ~5 mm. A 10-mm-diameter custom-designed cannulated end mill with a depth stop was placed over the K-wire, and a 2-mm-deep osteochondral defect was created on the dorsal, load-bearing aspect of the femoral head. The K-wire was only used during the drilling of the defect to stabilize the cannulated end mill and was then removed before placement of the implant. The osteochondral defect was then repaired with the cell-seeded scaffold (Fig. 1, H to L) in the implant group (Fig. 1K) and left empty in the control (empty defect) group (Fig. 1J). The fixation of the implant relied on an optimized press interference fit with the prepared defect; no sutures, fibrin glue, or other fasteners were used to stabilize the implant in the defect. The joint capsule was closed, and a prosthetic capsulorrhaphy was performed (*32*) using two 3.5-mm dorsally placed screws and two strands of fiber wire (Arthrex Inc., Naples, FL) placed in a figure-of-eight pattern around each screw and through a transosseous tunnel in the intertrochanteric area of the femur (Fig. 1L). The capsulorrhaphy was performed so as not to impair normal movement of the coxofemoral joint. The dogs were allowed unrestrained weight bearing and normal activity in their living areas for the first month. From the second month on, range of motion (ROM) and leash-walking exercises were instigated. In month 2 postoperatively, dogs received 5 min of leash walk and 30 cycles of ROM exercise on the operated hip joint twice daily. During months 3 to 6, dogs received 10 min of leash walk twice daily without any passive ROM exercises.

Outcome measures

Gait analysis

Kinetic gait analysis (*33*, *34*) was performed on trotting dogs using dual in-series force plates (Advanced Mechanical Technology Inc., Watertown, MA) preoperatively and every month following surgery. Velocity and acceleration were measured by means of five photometric switches that were connected to the computer analysis system and were kept within 1.7 to 2.1 m/s and ± 0.5 m/s^2, respectively. Five trials were collected from each dog at each time point. A single handler and computer operator performed all gait analysis throughout the study period. Specialized computer software (Sharon software,

Dewitt, MI) was used to calculate GRFs of the limbs. GRFs were expressed in percent body weight. PVF, VI, PPF, and PI were analyzed as previously demonstrated (*33*).

A pressure-sensitive walkway (7100 QL Virtual Sensor 4, Tekscan, Boston, MA) was used to measure static GRF data (body weight distribution) (*17*). Static data were acquired as previously described (*17*, *35*), preoperatively and every month postoperatively. For each dataset, the mean percentage body weight distribution through each limb over a steady 5-s period was recorded. Five replicates of pressure-sensitive walkway data were acquired for each animal per session (once per month) and used for analysis. GRFs (weight) were expressed in percent body weight distributed to that limb.

Actimetry

One triaxial, omnidirectional accelerometer (Actical, Philips Respironics, Bend, OR) was fixed onto the collar of each dog and worn throughout the study to continuously record activity and therefore translational movement (*25*). The recording epoch was set to 1 min, and data were downloaded every 4 weeks. Data for the 2 weeks before each outcome measure time point were extracted, and the activity over the 2-week period was calculated on a per-hour basis by the following equation

$$H_{\text{avg}} = \frac{\sum_{j=1}^{14}\left(\frac{\sum_{i=1}^{60} C_i}{60}\right)_j}{14}$$

where H_{avg} indicates average counts over a specific hour of the day over a 2-week period, and C_i indicates measured counts for each minute during the hour.

The times when dogs were removed from their cages for exercise were manually recorded cage-side, and activity data from these time periods were not included in the analysis. Thus, activity data only reflected spontaneous activity in the cage.

Radiography, ROM, and limb girth measurement

Standard extended ventro-dorsal and lateral coxofemoral joint radiographic views and distraction index views (*36*) were obtained on each animal preoperatively and every month for 6 months following surgery under sedation with dexmedetomidine (5 μg/kg, iv) and butorphanol (0.3 mg/kg, iv). All images were anonymized and randomly assigned an identification number using a free open source tool (DicomCleaner). The ventro-dorsal images were scored for severity of OA by two experienced blinded observers (consensus scoring), using an 11-point (0 to 10) numeric rating scale developed by the research team.

Cross-sectional area of the thigh via CT

Immediately before termination of the dogs, under sedation, CT images (SOMATOM Perspective 64, Siemens Medical Solutions USA Inc., Malvern, PA) were obtained of both hindlimbs from the cranial border of iliac wing to just distal to the toes using a slice thickness of 1 mm and spacing of 10 mm. Scan parameters were set at 120 to 130 kilovolt peak and 21 to 129 mA by using a 25-cm field of view, a 512 × 512 matrix. Cross-sectional area of the thigh was measured at the midpoint of the distance between the most proximal point of the greater trochanter and the midpoint of the lateral fabella using ImageJ (setting the lower and upper thresholds to −29 and +150). The difference in cross-sectional area (in square centimeters) between hindlimbs (operated minus unoperated) was calculated in each dog.

Joint motion and muscle circumference

At each data collection time point, circumference (girth) of each thigh was measured at point 70% of distance from the great trochanter to fabella in the standing dog using Gulick II tape measure (Country Technology Inc., Gays Mills, WI). Measurements were obtained in triplicate for each limb, and the mean value was used for analysis (*37*). The difference in the limb girth between hindlimbs was calculated (operated − unoperated).

Pain assessment

The CROPI-h (fig. S1), developed for the assessment of OA-associated pain and activity impairment in research dogs, was completed by a single observer for each dog preoperatively and every month postoperatively. A summed score (out of a total of 150) was assigned to each dog at each time point.

Histological assessment

Dogs were humanely terminated 6 months after surgery with an overdose of pentobarbital sodium and phenytoin sodium (Beuthanasia D solution, Schering-Plough Animal Health Corp., Union, NJ). Femora and acetabulae were harvested intact, wrapped in PBS-soaked gauze, and frozen (−20°C) until analysis.

Joint histology and immunohistochemistry

Implant and control osteochondral defects were transected with a low-speed diamond saw such that one-third of the osteochondral defect could be processed by decalcified histology and the other two-thirds of the defect could be processed by undecalcified histology and microradiography. Following decalcification, sections of tissue were stained with Alcian blue–periodic acid–Schiff, Safranin O/Fast Green, hematoxylin and eosin (H&E), and Mallory Aniline Blue connective tissue stain. For acetabula, only H&E decalcified histology was performed. For undecalcified histology, plastic-embedded tissue blocks were sectioned using low-speed diamond blades to an approximate thickness of 200 to 300 μm. Differential staining using a proprietary trichrome stain was performed to permit both histological and cytological differentiation. With this staining method, the following tissues can be differentiated on the basis of color: Bone is stained green, cartilage and fibrocartilage are stained dark purple, and fibrovascular tissue is stained pink.

For immunohistochemical analysis, antigen retrieval for sections labeled for type II collagen was performed using Digest-All (Life Technologies). Antigen retrieval for type I collagen slides was accomplished by submerging sections in pH 6.0 citrate buffer, and the buffer was brought to a boil in a microwave and then maintained at a sub-boiling temperature for 10 min. Monoclonal antibodies were used to identify type I collagen (diluted 1:400; rabbit anti–collagen I from Cell Signaling Technology, catalog no. 72026) and type II collagen (diluted 1:1; II-II6B3 from Developmental Studies Hybridoma Bank, University of Iowa, Iowa City, IA). The secondary antibody for type I collagen was the SignalStain Boost IHC Detection Reagent [horseradish peroxidase (HRP), rabbit] (Cell Signaling Technology, catalog no. 8114). For type II collagen, the secondary antibody was the SignalStain Boost IHC Detection Reagent (HRP, mouse) (Cell Signaling Technology, catalog no. 8125). Briefly, sections were covered with secondary solution (approximately 150 μl per section) and incubated with the secondary antibody solutions for 1 hour at room temperature. A DAB (3,3′-diaminobenzidine) chromogen was used for antigen labeling (DAB Substrate Kit, BD Pharmingen, catalog no. 550880).

A qualitative assessment of bone healing and cartilage repair was made within the osteochondral defects. In addition, a modified scoring system based on the O'Driscoll scale (*38*) (20 points in total) was used to evaluate all control femora and osteochondral defects. The O'Driscoll scale measured surface irregularity (3 points), cartilage level within the defect (2 points), bonding to adjacent cartilage (2 points),

regenerated subchondral bone (2 points), inflammatory cell inflammation around the implant (2 points), chondrocyte clustering (2 points), freedom from degenerative changes (3 points), and hyalinity (4 points).

Biochemical analysis

A section of day 0 constructs was removed and digested in papain for 12 hours at 58°C. DNA was measured using the Quant-iT PicoGreen dsDNA assay (Life Technologies). sGAG was measured using the dimethylmethylene blue assay using chondroitin 4-sulfate as a standard and reading the optical density on a plate reader (595 nm). For total collagen content, OHP was measured by hydrolyzing the digest in HCl and reacting the solution with *p*-dimethylaminobenzaldehyde and chloramine-T to measure OHP content per construct. Total collagen was then determined using 0.134 as the ratio of OHP to collagen (*18*).

Mechanical testing

Indentation testing was used to measure the compressive modulus of the articular cartilage of both the operated and contralateral control (unoperated) joints, as well as the day 0 implants. A minimum of three points were evaluated at the following locations: on the repair tissue, outside of the repair tissue on the treated limb, the contralateral control cartilage in the dorsal, load-bearing region, and on the articular surface of the day 0 implants. Indentation testing was performed using an ElectroForce testing instrument (TA Instruments, New Castle, DE), ensuring normality to the surface, and using a spherical 4-mm indenter to perform three compressive stress-relaxation steps at 5, 10, and 15% strain steps with a 10-min dwell following each step to allow the cartilage and de novo synthesized tissues to reach equilibrium. The resulting force-displacement data at 10% ε were then fit to a viscoelastic indentation model described by a modified Hertz equation (*39*, *40*) to determine the instantaneous and equilibrium modulus of the tissues.

Pathology assessment

Synovium samples were taken from dorsal, ventral, medial, and lateral sections of the operated and contralateral control joints to assess for inflammation. Briefly, the tissues were fixed in 10% neutral buffered formalin followed by processing for routine paraffin-embedded decalcified histology (*11*). All sections were stained with H&E and graded by a trained pathologist (D.J.V.) for chronic inflammation, synovial hyperplasia, and the presence of giant cells with a semi-quantitative four-point scoring system: normal, 0; mild, 1; moderate, 2; and severe, 3.

Statistical analysis

A longitudinal statistical analysis was performed to compare the two treatment groups across the postoperative time points. For the operated joint, d_{ijk} denotes the difference between the response at the kth time point ($k = 1,\ldots,6$) and its preoperative measurement for the jth subject ($j = 1,\ldots,6$) in the ith treatment group ($i = 1, 2$). The preoperative measurement is denoted x_{ij}. For all responses except the actimetry data, a two-way analysis of covariance (ANCOVA) model was used with responses d_{ijk}, covariate x_{ij}, and two factors: treatment and time. The treatment/time interaction effect was included in the model but removed when found to be statistically insignificant. The covariate effect was included because the range of values for d_{ijk} and the time required to return to baseline can depend on x_{ij}. A heterogenous, lag-1 autoregressive [abbreviated as AR(1)] covariance structure was assumed that allowed different variances for the six time points. For mechanical testing, the raw scores had large outliers, so two analysis approaches were taken: a two-sample t test using a log transformation and unequal variances and a non-parametric Wilcoxon test.

Analysis of the actimetry data was performed on d_{ijkl}, the lth hourly difference between the measurements at time point k and the preoperative measurements, x_{ijl}. A three-way ANCOVA mixed model was fitted, having all main and two-way interactions between the factors treatment, time point, and hour as fixed effects and random effects for each subject as well as the subject/time point interaction effects. The subject/time point interaction random effects were assigned a homogenous, AR(1) covariance structure, while the residual effects were assumed to have a heterogeneous, AR(1) covariance structure.

For each response, we first fit the interaction model described above. If the interaction effect was significant, then we reported which time points exhibited significant differences between the treatment groups and their effect sizes. If the time point/treatment interaction effects were insignificant, then the effects were dropped from the model, but all other effects were left in the model regardless of their statistical significance. Analyses were performed using PROC MIXED in SAS 9.4. Statistical tests were performed using the Kenward-Roger denominator degrees of freedom method. Statistical significance was based on a significance level of 0.05. Post hoc comparisons that were performed using Tukey adjustments were used to correct for multiple testing.

SUPPLEMENTARY MATERIALS

Supplementary material for this article is available at https://science.org/doi/10.1126/sciadv.abi5918

View/request a protocol for this paper from *Bio-protocol*.

REFERENCES AND NOTES

1. J. D. Keener, J. J. Callaghan, D. D. Goetz, D. R. Pederson, P. M. Sullivan, R. C. Johnston, Twenty-five-year results after charnley total hip arthroplasty in patients less than fifty years old—A concise follow-up of a previous report. *J. Bone Joint Surg. Am. Vol.* **85A**, 1066–1072 (2003).
2. L. Hangody, J. Dobos, E. Balo, G. Panics, L. R. Hangody, I. Berkes, Clinical experiences with autologous osteochondral mosaicplasty in an athletic population: A 17-year prospective multicenter study. *Am. J. Sports Med.* **38**, 1125–1133 (2010).
3. D. B. Saris, J. Vanlauwe, J. Victor, K. F. Almqvist, R. Verdonk, J. Bellemans, F. P. Luyten; TIG/ACT/01/2000&EXT Study Group, Treatment of symptomatic cartilage defects of the knee: Characterized chondrocyte implantation results in better clinical outcome at 36 months in a randomized trial compared to microfracture. *Am. J. Sports Med.* **37** (Suppl. 1), 10S–19S (2009).
4. G. Filardo, F. Vannini, M. Marcacci, L. Andriolo, A. Ferruzzi, S. Giannini, E. Kon, Matrix-assisted autologous chondrocyte transplantation for cartilage regeneration in osteoarthritic knees: Results and failures at midterm follow-up. *Am. J. Sports Med.* **41**, 95–100 (2013).
5. P. Niemeyer, P. Lenz, P. C. Kreuz, G. M. Salzmann, N. P. Sudkamp, H. Schmal, M. Steinwachs, Chondrocyte-seeded type I/III collagen membrane for autologous chondrocyte transplantation: Prospective 2-year results in patients with cartilage defects of the knee joint. *Art Ther.* **26**, 1074–1082 (2010).
6. T. Minas, A. H. Gomoll, S. Solhpour, R. Rosenberger, C. Probst, T. Bryant, Autologous chondrocyte implantation for joint preservation in patients with early osteoarthritis. *Clin. Orthop. Relat. Res.* **468**, 147–157 (2010).
7. P. K. Valonen, F. T. Moutos, A. Kusanagi, M. G. Moretti, B. O. Diekman, J. F. Welter, A. I. Caplan, F. Guilak, L. E. Freed, In vitro generation of mechanically functional cartilage grafts based on adult human stem cells and 3D-woven poly(epsilon-caprolactone) scaffolds. *Biomaterials* **31**, 2193–2200 (2010).
8. P. H. Ousema, F. T. Moutos, B. T. Estes, A. I. Caplan, D. P. Lennon, F. Guilak, J. B. Weinberg, The inhibition by interleukin 1 of MSC chondrogenesis and the development of biomechanical properties in biomimetic 3D woven PCL scaffolds. *Biomaterials* **33**, 8967–8974 (2012).
9. F. T. Moutos, L. E. Freed, F. Guilak, A biomimetic three-dimensional woven composite scaffold for functional tissue engineering of cartilage. *Nat. Mater.* **6**, 162–167 (2007).

10. F. T. Moutos, F. Guilak, Functional properties of cell-seeded three-dimensionally woven poly(epsilon-caprolactone) scaffolds for cartilage tissue engineering. *Tissue Eng. Part A* **16**, 1291–1301 (2009).
11. F. T. Moutos, K. A. Glass, S. A. Compton, A. K. Ross, C. A. Gersbach, F. Guilak, B. T. Estes, Anatomically shaped tissue-engineered cartilage with tunable and inducible anticytokine delivery for biological joint resurfacing. *Proc. Natl. Acad. Sci. U.S.A.* **113**, E4513–E4522 (2016).
12. B. L. Larson, S. N. Yu, H. Park, B. T. Estes, F. T. Moutos, C. J. Bloomquist, P. B. Wu, J. F. Welter, R. Langer, F. Guilak, L. E. Freed, Chondrogenic, hypertrophic, and osteochondral differentiation of human mesenchymal stem cells on three-dimensionally woven scaffolds. *J. Tissue Eng. Regen. Med.* **13**, 1453–1465 (2019).
13. F. T. Moutos, B. T. Estes, F. Guilak, Multifunctional hybrid three-dimensionally woven scaffolds for cartilage tissue engineering. *Macromol. Biosci.* **10**, 1355–1364 (2010).
14. E. Ko, S. W. Cho, Biomimetic polymer scaffolds to promote stem cell-mediated osteogenesis. *Int. J. Stem Cells* **6**, 87–91 (2013).
15. D. Little, S. Johnson, J. Hash, S. A. Olson, B. T. Estes, F. T. Moutos, B. D. Lascelles, F. Guilak, Functional outcome measures in a surgical model of hip osteoarthritis in dogs. *J. Exp. Orthop.* **3**, 17 (2016).
16. C. Pascual-Garrido, F. Guilak, M. F. Rai, M. D. Harris, M. J. Lopez, R. J. Todhunter, J. C. Clohisy, Canine hip dysplasia: A natural animal model for human developmental dysplasia of the hip. *J. Orthop. Res.* **36**, 1807–1817 (2018).
17. B. D. Lascelles, M. Freire, S. C. Roe, V. DePuy, E. Smith, D. J. Marcellin-Little, Evaluation of functional outcome after BFX total hip replacement using a pressure sensitive walkway. *Vet. Surg.* **39**, 71–77 (2010).
18. J. F. Woessner Jr., The determination of hydroxyproline in tissue and protein samples containing small proportions of this imino acid. *Arch. Biochem. Biophys.* **93**, 440–447 (1961).
19. S. C. Budsberg, J. N. Chambers, S. L. Lue, T. L. Foutz, L. Reece, Prospective evaluation of ground reaction forces in dogs undergoing unilateral total hip replacement. *Am. J. Vet. Res.* **57**, 1781–1785 (1996).
20. J. S. Bahl, M. J. Nelson, M. Taylor, L. B. Solomon, J. B. Arnold, D. Thewlis, Biomechanical changes and recovery of gait function after total hip arthroplasty for osteoarthritis: A systematic review and meta-analysis. *Osteoarthr. Cartil.* **26**, 847–863 (2018).
21. A. V. Wiik, A. Aqil, M. Brevadt, G. Jones, J. Cobb, Abnormal ground reaction forces lead to a general decline in gait speed in knee osteoarthritis patients. *World J. Orthop.* **8**, 322–328 (2017).
22. R. Seibert, D. J. Marcellin-Little, S. C. Roe, V. DePuy, B. D. Lascelles, Comparison of body weight distribution, peak vertical force, and vertical impulse as measures of hip joint pain and efficacy of total hip replacement. *Vet. Surg.* **41**, 443–447 (2012).
23. M. G. Conzemius, J. Vandervoort, Total joint replacement in the dog. *Vet. Clin. North Am. Small Anim. Pract.* **35**, 1213–1231, vii (2005).
24. V. L. Talis, A. A. Grishin, I. A. Solopova, T. L. Oskanyan, V. E. Belenky, Y. P. Ivanenko, Asymmetric leg loading during sit-to-stand, walking and quiet standing in patients after unilateral total hip replacement surgery. *Clin. Biomech.* **23**, 424–433 (2008).
25. B. D. Hansen, B. D. Lascelles, B. W. Keene, A. K. Adams, A. E. Thomson, Evaluation of an accelerometer for at-home monitoring of spontaneous activity in dogs. *Am. J. Vet. Res.* **68**, 468–475 (2007).
26. B. D. Lascelles, D. Knazovicky, B. Case, M. Freire, J. F. Innes, A. C. Drew, D. P. Gearing, A canine-specific anti-nerve growth factor antibody alleviates pain and improves mobility and function in dogs with degenerative joint disease-associated pain. *BMC Vet. Res.* **11**, 101 (2015).
27. A. Holsgaard-Larsen, E. M. Roos, Objectively measured physical activity in patients with end stage knee or hip osteoarthritis. *Eur. J. Phys. Rehabil. Med.* **48**, 577–585 (2012).
28. A. Grimaldi, C. Richardson, G. Durbridge, W. Donnelly, R. Darnell, J. Hides, The association between degenerative hip joint pathology and size of the gluteus maximus and tensor fascia lata muscles. *Man. Ther.* **14**, 611–617 (2009).
29. H. Sun, L. Mei, C. Song, X. Cui, P. Wang, The in vivo degradation, absorption and excretion of PCL-based implant. *Biomaterials* **27**, 1735–1740 (2006).
30. M.-H. Huang, S. M. Li, D. W. Hutmacher, J. Coudane, M. Vert, Degradation characteristics of poly(ε-caprolactone)-based copolymers and blends. *J. Appl. Polym. Sci.* **102**, 1681–1687 (2006).
31. P. Yilgor, R. A. Sousa, R. L. Reis, N. Hasirci, V. Hasirci, 3D plotted PCL scaffolds for stem cell based bone tissue engineering. *Macromol. Symp.* **269**, 92–99 (2008).
32. M. E. Johnson, T. D. Braden, A retrospective study of prosthetic capsule technique for the treatment of problem cases of dislocated hips. *Vet. Surg.* **16**, 346–351 (1987).
33. B. D. Lascelles, S. C. Roe, E. Smith, L. Reynolds, J. Markham, D. Marcellin-Little, M. S. Bergh, S. C. Budsberg, Evaluation of a pressure walkway system for measurement of vertical limb forces in clinically normal dogs. *Am. J. Vet. Res.* **67**, 277–282 (2006).
34. S. C. Budsberg, S. A. Johnston, P. D. Schwarz, C. E. DeCamp, R. Claxton, Efficacy of etodolac for the treatment of osteoarthritis of the hip joints in dogs. *J. Am. Vet. Med. Assoc.* **214**, 206–210 (1999).
35. A. Tomas, D. Bledsoe, S. Wall, G. Davidson, B. D. Lascelles, Initial evaluation of a canine stifle arthrotomy post-operative pain model. *Vet. J.* **204**, 293–298 (2015).
36. G. K. Smith, D. N. Biery, T. P. Gregor, New concepts of coxofemoral joint stability and the development of a clinical stress-radiographic method for quantitating hip joint laxity in the dog. *J. Am. Vet. Med. Assoc.* **196**, 59–70 (1990).
37. W. I. Baltzer, S. Smith-Ostrin, J. J. Warnock, C. G. Ruaux, Evaluation of the clinical effects of diet and physical rehabilitation in dogs following tibial plateau leveling osteotomy. *J. Am. Vet. Med. Assoc.* **252**, 686–700 (2018).
38. S. W. O'Driscoll, R. G. Marx, D. E. Beaton, Y. Miura, S. H. Gallay, J. S. Fitzsimmons, Validation of a simple histological-histochemical cartilage scoring system. *Tissue Eng.* **7**, 313–320 (2001).
39. J. W. Harding, I. N. Sneddon, The elastic stresses produced by the indentation of the plane surface of a semi-infinite elastic solid by a rigid punch. *Math. Proc. Camb. Philos. Soc.* **41**, 16–26 (1945).
40. E. M. Darling, S. Zauscher, F. Guilak, Viscoelastic properties of zonal articular chondrocytes measured by atomic force microscopy. *Osteoarthr. Cartil.* **14**, 571–579 (2006).

Acknowledgments: We would like to acknowledge I. Bukovnik for diligent animal care and S. Wall for technical assistance. We also acknowledge S. Compton for work culturing the MSCs in this study, T. Buford for the histological processing, and S. Oswald for excellent editorial work on the manuscript. **Funding:** Research reported in this publication was supported by Shriners Hospitals for Children, the Arthritis Foundation, the Nancy Taylor Foundation for Chronic Diseases, and the NIH (AR055042, AG46927, AG15768, AR74240, AR073752, and AR074992). The content is solely the responsibility of the authors and does not necessarily represent the official views of the NIH. **Author contributions:** M.E. assisted in surgeries, performed animal evaluations and data collection, coordinated the study, and performed data analysis. B.T.E. and F.T.M. conceived and planned the study, preparation of implant and cell culture, and data analysis. M.A.C. assisted in data collection and animal evaluations. J.S. and B.T.E. performed statistical analyses. D.L. conceived the study, helped to plan the study, and assisted in surgery. F.G. conceived the study, participated in its design and data interpretation, and participated in manuscript preparation. J.M.T. and P.E. prepared the joint tissues for histology and performed the histopathological analysis. D.J.V. performed the pathology analysis of synovial tissue and remote organs. B.D.X.L. planned the study and details of outcome measure collection, performed surgeries, trained personnel, oversaw all aspects of the in vivo work and data collection, and participated in manuscript preparation. All authors read and approved the final manuscript. **Competing interests:** M.E., M.A.C., S. J. Wall, J.S., and B.D.X.L. declare that they have no competing interests. D.L. is a paid consultant for Cytex Therapeutics Inc. F.G., F.T.M., V.P.W., and B.T.E. are employees and shareholders of Cytex Therapeutics Inc. F.G., F.T.M., and B.T.E. are inventors on patents filed by Cytex Therapeutics Inc. relating to the contents of this work (#8,691,542; #9,649,409: filed 7 April 2014, awarded 16 May 2017; #10,022,231: filed 7 October 2016, awarded 17 July 2018; and #10,940,007: filed 7 October 2016, awarded 2 March 2021). The authors declare that they have no other competing interests. **Data and materials availability:** All data needed to evaluate the conclusions in the paper are present in the paper and/or the Supplementary Materials.

Submitted 18 March 2021
Accepted 22 July 2021
Published 15 September 2021
10.1126/sciadv.abi5918

Citation: B. T. Estes, M. Enomoto, F. T. Moutos, M. A. Carson, J. M. Toth, P. Eggert, J. Stallrich, V. P. Willard, D. J. Veis, D. Little, F. Guilak, B. D. X. Lascelles, Biological resurfacing in a canine model of hip osteoarthritis. *Sci. Adv.* **7**, eabi5918 (2021).

ScienceAdvances

Biological resurfacing in a canine model of hip osteoarthritis

Bradley T. EstesMasataka EnomotoFranklin T. MoutosMegan A. CarsonJeffrey M. TothPeter EggertJonathan StallrichVincent P. WillardDeborah J. VeisDianne LittleFarshid GuilakB. Duncan X. Lascelles

Sci. Adv., 7 (38), eabi5918. • DOI: 10.1126/sciadv.abi5918

Science Advances (ISSN) is published by the American Association for the Advancement of Science. 1200 New York Avenue NW, Washington, DC 20005. The title *Science Advances* is a registered trademark of AAAS.